Title
Tissue-specific pathways extrude activated ILC2s to disseminate type 2 immunity

Permalink
https://escholarship.org/uc/item/7wm5s15x

Journal
Journal of Experimental Medicine, 217(4)

ISSN
0022-1007

Authors
Ricardo-Gonzalez, Roberto R
Schneider, Christoph
Liao, Chang
et al.

Publication Date
2020-04-06

DOI
10.1084/jem.20191172

Peer reviewed

Tissue-specific pathways extrude activated ILC2s to disseminate type 2 immunity

Roberto R. Ricardo-Gonzalez[1]* ⓘ, Christoph Schneider[2]* ⓘ, Chang Liao[2], Jinwoo Lee[2] ⓘ, Hong-Erh Liang[2] ⓘ, and Richard M. Locksley[2,3,4] ⓘ

Group 2 innate lymphoid cells (ILC2s) are tissue-resident cells prominent at barrier sites. Although precursors are found in blood, mature ILC2s can enter the circulation after small intestinal perturbation by migratory helminths and move to distant tissues to influence the local reparative response. Using fate-mapping and methods to bypass the lung or intestinal phases of *Nippostrongylus brasiliensis* infection, we show that blood ILC2s comprise heterogeneous populations derived from distinct tissues that are dependent on alarmins matched to the receptor profile of the specific tissue ILC2s. Activation of local ILC2s by tissue-specific alarmins induced their proliferation, lymph node migration, and blood dissemination, thus systemically distributing type 2 cytokines. These studies uncover a possible mechanism by which local innate responses transition to systemic type 2 responses by extrusion of activated sentinel ILC2s from tissue into the circulation.

Introduction

Prevalent at tissue barriers, group 2 innate lymphoid cells (ILC2s) comprise a population of lymphocytes with the capacity to generate a spectrum of cytokines associated with allergic immunity (Vivier et al., 2018) and are implicated in metabolic and regenerative responses linked with homeostasis, growth, and injury (Kotas and Locksley, 2018). Although precise mechanisms remain incompletely defined, dysregulated tissue ILC2 responses are associated with increasingly prevalent allergic diseases, and further understanding is needed to enable potential therapeutic opportunities for enabling or disabling these cells as well as T helper type 2 cells with similar properties (Cherrier et al., 2018; Van Dyken et al., 2016) in order to sustain tissue homeostasis and control allergic pathology.

ILC2s are distributed into tissues during a perinatal window where they undergo marked proliferation and take on transcriptomic signatures associated with their tissues of residence (Schneider et al., 2019). At homeostasis, tissue ILC2s are tissue-resident and presumably self-renewing, as assessed by studies using parabiotic animals (Gasteiger et al., 2015; Huang et al., 2018; Moro et al., 2016; Schneider et al., 2019). Consistent with a self-renewing tissue-resident population, there is relatively low engraftment of donor ILC2s in host tissues after hematopoietic stem cell transplantation (Vély et al., 2016). However, circulating ILC precursors can be recovered from the blood of mice and humans (Bar-Ephraim et al., 2019; Lim et al., 2017);

slow turnover occurs as shown by the gradual replacement of fate-mapped ILC2s in mice (Schneider et al., 2019), suggesting that tissue cells can be replenished from an immature precursor, whether from the bone marrow (BM) or elsewhere (Ghaedi et al., 2016).

Recently, blood ILC2s were shown to increase substantially in mice after infection with the migratory helminth *Nippostrongylus brasiliensis* (Huang et al., 2018). Blood ILC2s were attributed to being from the small intestine by their stable expression of the IL-25 receptor component IL-17RB and by the ability of exogenous IL-25 to mobilize small intestinal ILC2s into the bloodstream through an activation-dependent process related to expression of S1P receptors and exit from the lamina propria (Huang et al., 2018). ILC2s have also been proposed to egress from the BM to fuel expanding ILC2 tissue pools in mice that were treated with IL-33 or after fungal aeroallergen challenge (Karta et al., 2018; Stier et al., 2018). By using the site-specific signatures of resident ILC2s in different tissues together with fate-mapping and by varying the route and timing of infection, we were able to identify the tissue origins of ILC2s that appear in the blood after infection with *N. brasiliensis*. We uncovered tissue-specific mechanisms by which activated ILC2s enter the blood by extrusion from perturbed tissues and thus transition from local enforcers of homeostasis to systemic arbiters of type 2 immunity.

[1]Department of Dermatology, University of California, San Francisco, San Francisco, CA; [2]Department of Medicine, University of California, San Francisco, San Francisco, CA; [3]Department of Microbiology and Immunology, University of California, San Francisco, San Francisco, CA; [4]Howard Hughes Medical Institute, University of California, San Francisco, San Francisco, CA.

*R.R. Ricardo-Gonzalez and C. Schneider contributed equally to this work; Correspondence to Richard M. Locksley: richard.locksley@ucsf.edu; C. Schneider's present address is Institute of Physiology, University of Zurich, Zurich, Switzerland.

Check for updates

Results and discussion

Circulating ILC2s phenotypically differ during the course of *N. brasiliensis* infection

Although most ILC2s are resident in peripheral tissues, activation of small intestinal ILC2s after helminth infection or in response to exogenous IL-25 enhanced their migratory behavior, resulting in their appearance in the blood (Huang et al., 2018). We performed a kinetic analysis of blood ILC2s following infection with the migratory helminth *N. brasiliensis* using reporter mice for Arg1, IL-5, and IL-13 (YRS), which facilitates identification of ILC2s and their activation status in situ (Liang et al., 2011; Nussbaum et al., 2013). Blood ILC2s, identified based on IL-5 reporter expression among lineage-negative cells, were rare to undetectable in naive mice and during the first 3 d after infection with *N. brasiliensis* (Fig. 1, A and B; and Fig. S1). IL-5$^+$KLRG1$^+$ ILC2s appeared in the blood by day 5 (d5) after infection and remained high for the next 7–10 d before returning to baseline. On d5, these cells displayed a KLRG1$^+$IL-17RB$^+$ST2$^-$Arg1$^-$ phenotype that resembled tissue-resident ILC2s in resting small intestinal lamina propria (Fig. 1 A). Over time, this phenotype changed to a KLRG1$^+$IL-17RB^{int}ST2$^+$Arg1$^+$ expression profile, which resembled tissue-resident ILC2s in resting lung (Fig. 1 A). Notably, circulating ILC2s on d5 and d12 expressed IL-13, a dynamic marker of ILC2 activation (Fig. 1, C and D); IL-13 evels were higher among the d5 IL-17RB$^+$ST2$^-$ ILC2s and similar to that of ILC2s with the same phenotype that had accumulated in the lung at this time point. Blood levels of IL-13 after *N. brasiliensis* infection closely matched the presence of blood IL-13 reporter-positive ILC2s in the blood, the dominant source of IL-13 in the circulation (Fig. S2 A), consistent with a mechanism by which innate allergic cytokines can mediate systemic effects before the onset of adaptive type 2 immunity (Fig. 1 E). Administration of FTY720 during *N. brasiliensis* infection resulted in marked reduction of circulating ILC2s throughout the course of the infection (Fig. 2, A–F). Blockade of ILC2 entry into the circulation using FTY720 resulted in reduction of serum IL-13 (Fig. 1 E) and a reduction in dividing IL-13$^+$ ILC2s from the blood on d5 (Fig. S2 B). Before and after infection, lung ILC2s were largely ST2$^+$Arg1$^+$, although a proportion of activated ST2$^-$IL-17RB$^+$CD69$^-$ ILC2s became apparent on d5, consistent with previous observations (Huang et al., 2015; Fig. 1, A and D); these cells were readily labeled with i.v. injected anti-CD45 antibody and were markedly reduced in the setting of FTY720, consistent with their residence in lung vasculature rather than parenchymal tissue (Fig. 2, C and D; and Fig. S2, C and D). These results suggest unappreciated diversity in circulating ILC2s, which likely derive from multiple sources, including the lung and the small intestine, which are the main sites of tissue perturbation by the migratory helminth (Bouchery et al., 2017).

Cytokine-dependent ILC2 activation drives distinct waves of blood ILC2s

Based on the phenotypic differences in ST2 and IL-17RB cytokine receptor expression on lung and small intestine ILC2s, respectively (Ricardo-Gonzalez et al., 2018), we hypothesized that these temporally distinct circulating ILC2s might have been elicited from tissues by their specific cytokine ligands, IL-33 and IL-25, which can provide redundant signals during the course of *N. brasiliensis* infection (Neill et al., 2010). To test this, we used IL-25–deficient (*Il25$^{-/-}$*) and ST2-deficient (ST2$^{-/-}$) mice and assessed whether these cytokine signaling pathways were required during the appearance of blood ILC2s. Notably, d5 blood ILC2s were significantly reduced in mice deficient in IL-25 (Fig. 3 A), a cytokine potent in activating small intestinal ILC2s (Schneider et al., 2018; von Moltke et al., 2016), and the remaining were predominantly of ST2$^+$ phenotype (Fig. 3 B). Of note, the percentages of blood ILC2s on d12 were not diminished when comparing *Il25$^{-/-}$* and WT mice (Fig. 3 C). In contrast, loss of IL-33 signaling in ST2$^{-/-}$ mice did not alter the accumulation of d5 blood ILC2s, but it significantly reduced the blood ILC2s on d12 (Fig. 3, A and C). Indeed, these defects were mirrored in the lung: the accumulation of IL-17RB^{hi}ST2$^-$Arg1$^-$ ILC2s in the lung, as well as IL-13–expressing ILC2s, was absent in IL-25–deficient mice on d5 but normal in ST2-deficient mice (Fig. 3, D–G). However, the overall increase in lung ILC2s, which was largely driven by an expansion of resident IL-17RB^{low}ST2$^+$Arg1$^+$ ILC2s, was abrogated in *ST*2-deficient mice but not in *Il25$^{-/-}$* mice (Fig. 3, D–G). We observed similar dynamics when examining the mesenteric lymph node (mLN), a proxy for small intestinal lamina propria cells in the infected state (Fig. 3 H). Taken together, our findings suggest temporally and spatially distinct roles for these two cytokines in ILC2 activation and blood invasion, in which IL-25–dependent small intestinal ILC2s generate an early wave of circulating ILC2s (d5) that becomes replaced by an IL-33–dependent late wave of blood ILC2s that likely originates from the lung (d12).

Using fate-mapping to trace the tissue of origin of circulating ILC2s

Based on our results, we hypothesized that circulating ILC2s during *N. brasiliensis* infection might be of dual origin, consisting of an early wave appearing on d5 that originates from the small intestine and a subsequent wave appearing on d10–d12 that originates from the lung. To more precisely localize the tissues of origin for these ILC2 populations, we made use of a recently described *Arg1*-CreERT2 fate-mapping approach (Schneider et al., 2019; Fig. 4 A). In this system, ILC2s are fate-mapped using tamoxifen among groups of mice during the first 2 wk after birth and then maintained without tamoxifen for 10 wk. Due to differences in dilution of resident ILC2s among tissues (Schneider et al., 2019), tissue ILC2s from the adult mice differ in their labeling frequencies; the lung sustained a high prevalence of fate-mapped cells (60%) compared with only 15% among small intestinal lamina propria ILC2s; ILC2s in the BM were almost fully diluted of fate-mapped cells over this time (Fig. 4 B and Fig. S3 A). 3 wk after infection with *N. brasiliensis*, these organ-specific labeling frequencies remained relatively constant in tissues (Fig. 4 B). Although ILC2 numbers significantly increased in the lung and small intestinal lamina propria through the course of the infection, the ratios of fate-mapped versus non–fate-mapped cells in the lung, small intestine, and BM were
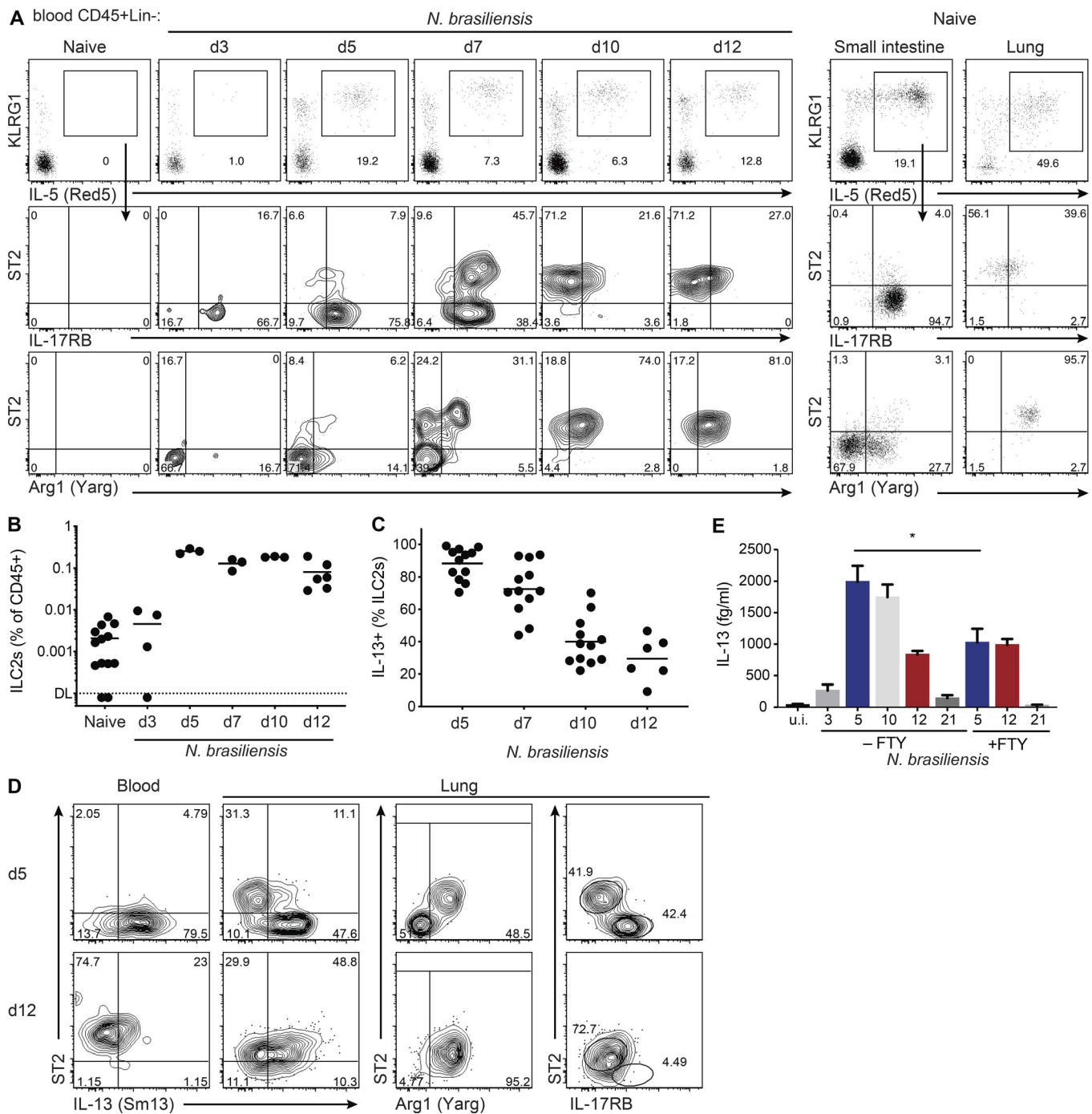
Ricardo-Gonzalez et al.
Niche extrusion of tissue ILC2s into circulation

Journal of Experimental Medicine   2 of 12
https://doi.org/10.1084/jem.20191172

Figure 1. **Circulating ILC2s phenotypically differ during the course of *N. brasiliensis* infection. (A–D)** *Arg1*[Yarg]*Il5*[Red5]*Il13*[Sm13] (YRS) triple-reporter mice were infected with *N. brasiliensis* and analyzed at the indicated time points. Uninfected mice (Naive) were examined as controls. **(A)** Expression of KLRG1 and IL-5 by cells gated on CD45+Lin− cells isolated from peripheral blood (left) or small intestine lamina propria and lung (right). Expression of ST2 and IL-17RB or Arg1 by ILC2s gated as indicated in the top panels. **(B and C)** Frequencies of KLRG1+IL-5 (Red5)+ ILC2s (B) and percentages of IL-13 reporter–positive ILC2s (C) in peripheral blood. DL, detection limit. **(D)** Flow cytometry plots of blood (left) or lung (right) ILC2s gated on CD45+Lin−IL-5+ cells from d5 or d12, highlighting activation as assessed by IL-13 (Sm13) expression and the expression of ST2, Arg1 (Yarg), and IL-17RB. **(E)** Serum IL-13 levels from WT C57BL/6J mice infected with *N. brasiliensis* treated with or without FTY720 (FTY) and analyzed at the indicated time points. The x axis represents days after infection. Data displayed as mean ± SEM. u.i., uninfected. Data are from one experiment representative of at least two independent experiments (A, D, and E) or pooled from multiple independent experiments (B and C). *, P < 0.05.
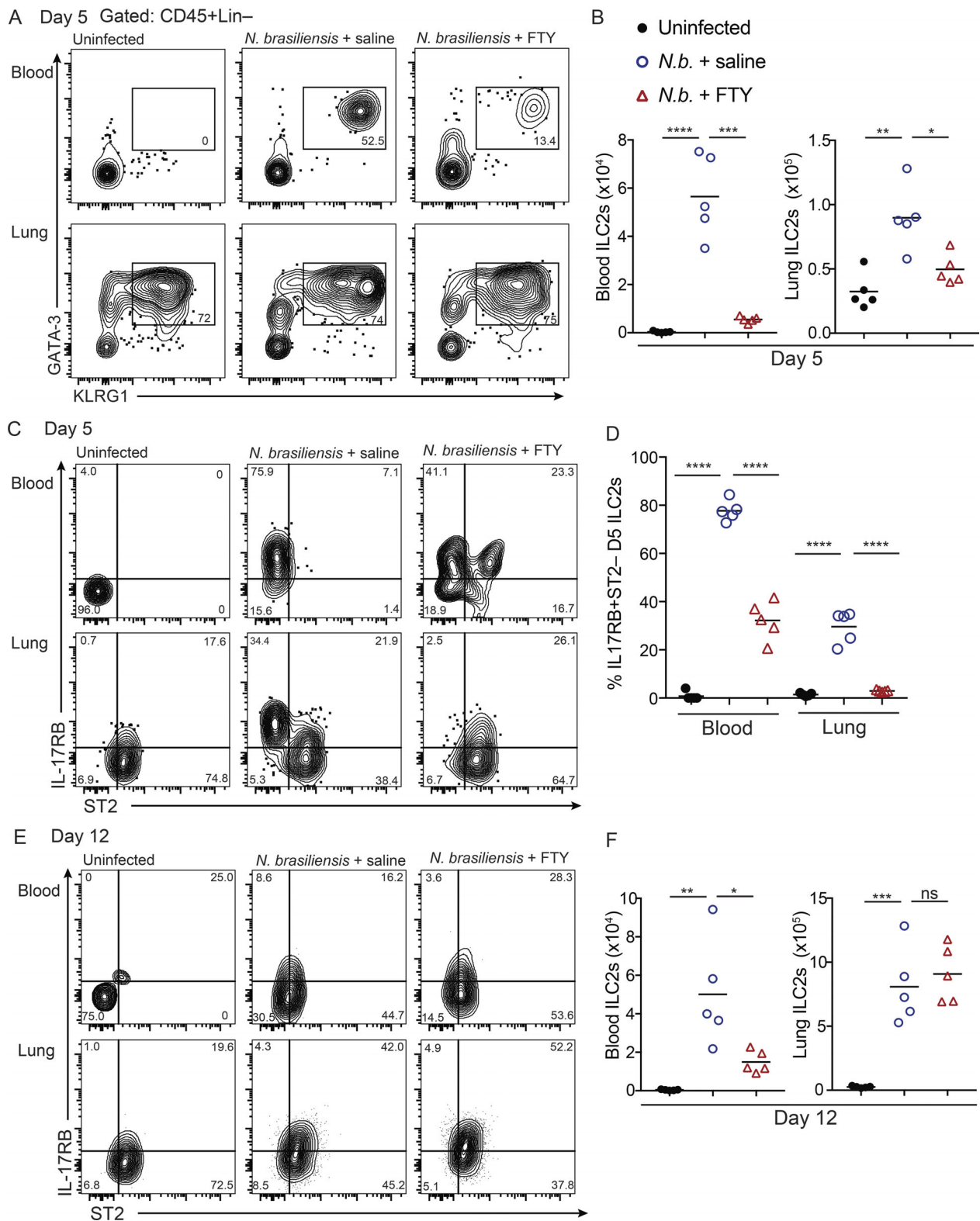
Ricardo-Gonzalez et al.
Niche extrusion of tissue ILC2s into circulation

Journal of Experimental Medicine   3 of 12
https://doi.org/10.1084/jem.20191172

Figure 2. **Circulating ILC2s are dependent on tissue extrusion. (A–H)** C57BL/6J mice were infected with *N. brasiliensis*, injected i.p. with saline or FTY720 (1 mg/kg daily from day of infection), and analyzed at the indicated time points. **(A)** Gating of ILC2s (pregated on live CD45$^+$Lin$^-$) from blood or lung. **(B)** Total number of ILC2s in the blood (left) or lung (right) at d5. **(C–E)** Flow cytometry plots showing the expression of ST2 and IL-17RB on blood and lung ILC2s from d5 (C) and d12 (E) and quantification of the percentage of IL-17RB$^+$ST2$^-$ ILC2s in the blood and lung on d5 (D). **(F)** Total number of ILC2s in the blood (left) or lung (right) at d12. Data are representative of two independent experiments with *n* ≥ 3 individual mice per group. *, P < 0.05; **, P < 0.005; ***, P < 0.0005; ****, P < 0.0001. *N.b.*, *N. brasiliensis*; ns, no significant difference.
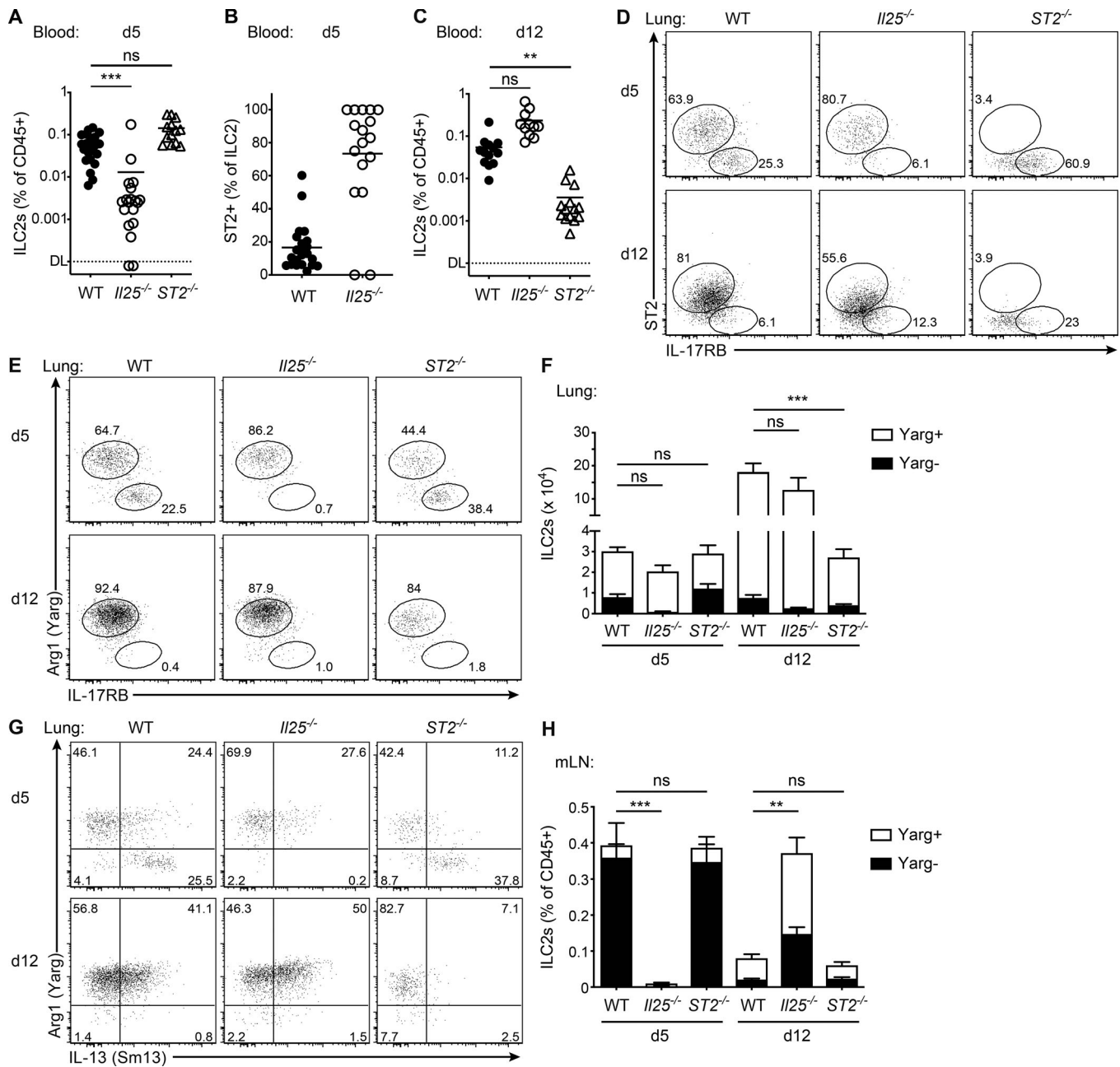
Figure 3. **Differential cytokine-dependent tissue ILC2 activation correlates with appearance of ILC2s. (A–H)** WT, *Il25*^{−/−}, or *Il1rl1*^{−/−} (*ST2*^{−/−}) mice on *Arg1*[Yarg]*Il5*[Red5]*Il13*[Sm13] triple-reporter strain were infected with *N. brasiliensis* and analyzed on d5 and d12. **(A)** Quantification of KLRG1^{+}IL-5 (Red5)[+] blood ILC2s as a percentage of CD45^{+} cells on d5. DL, detection limit. **(B)** Percentages of ST2^{+} cells among KLRG1^{+}IL-5^{+} blood ILC2s on d5. **(C)** Quantification of KLRG1^{+}IL-5^{+} blood ILC2s as percentage of CD45^{+} cells on d12. **(D)** Expression of ST2 and IL-17RB by ILC2s gated on Lin^{−}CD45^{+}IL-5^{+} cells isolated from the lung on d5 and d12. **(E)** Expression of Arg1 and IL-17RB by ILC2s gated on Lin^{−}CD45^{+}IL-5^{+} cells isolated from the lung on d5 and d12. **(F and G)** Quantification of total IL-5^{+}Arg1^{+} and Arg1^{−} ILC2s in the lung (F) and their expression of IL-13 (Sm13; G) on d5 and d12. **(H)** Frequencies of IL-5^{+}Arg1^{+} and IL-5^{+}Arg1^{−} ILC2s in the mLN. Data are pooled from multiple independent experiments and displayed as mean ± SEM of 11–14 individual mice per group and time point (A–C, F, and H) or from one experiment representative of at least three independent experiments (D, E, and G). **, P < 0.005; ***, P < 0.0005. ns, no significant difference.

largely maintained, corroborating the stability of the individual local ILC2 tissue pools (Fig. 4, C and D; and Fig. S3 B); however, a slight but significant dilution in labeling was noted in the lung at d5, whereas KLRG1^{+} (activated)-labeled BM ILC2s increased (Fig. 4, C and E). In contrast to the relatively stable tissue ILC2 pools throughout the infection, circulating ILC2s in the blood differed markedly in the percentage of fate-mapped cells between d5 and d12, thus indicating their origin from different tissues. Indeed, consistent with their surface marker phenotype, the percentage of fate-mapped blood ILC2s on d5 closely matched the percentage of fate-mapped ILC2s in the small intestine (Fig. 4 F and Fig. S3 C) and was also similar to that of
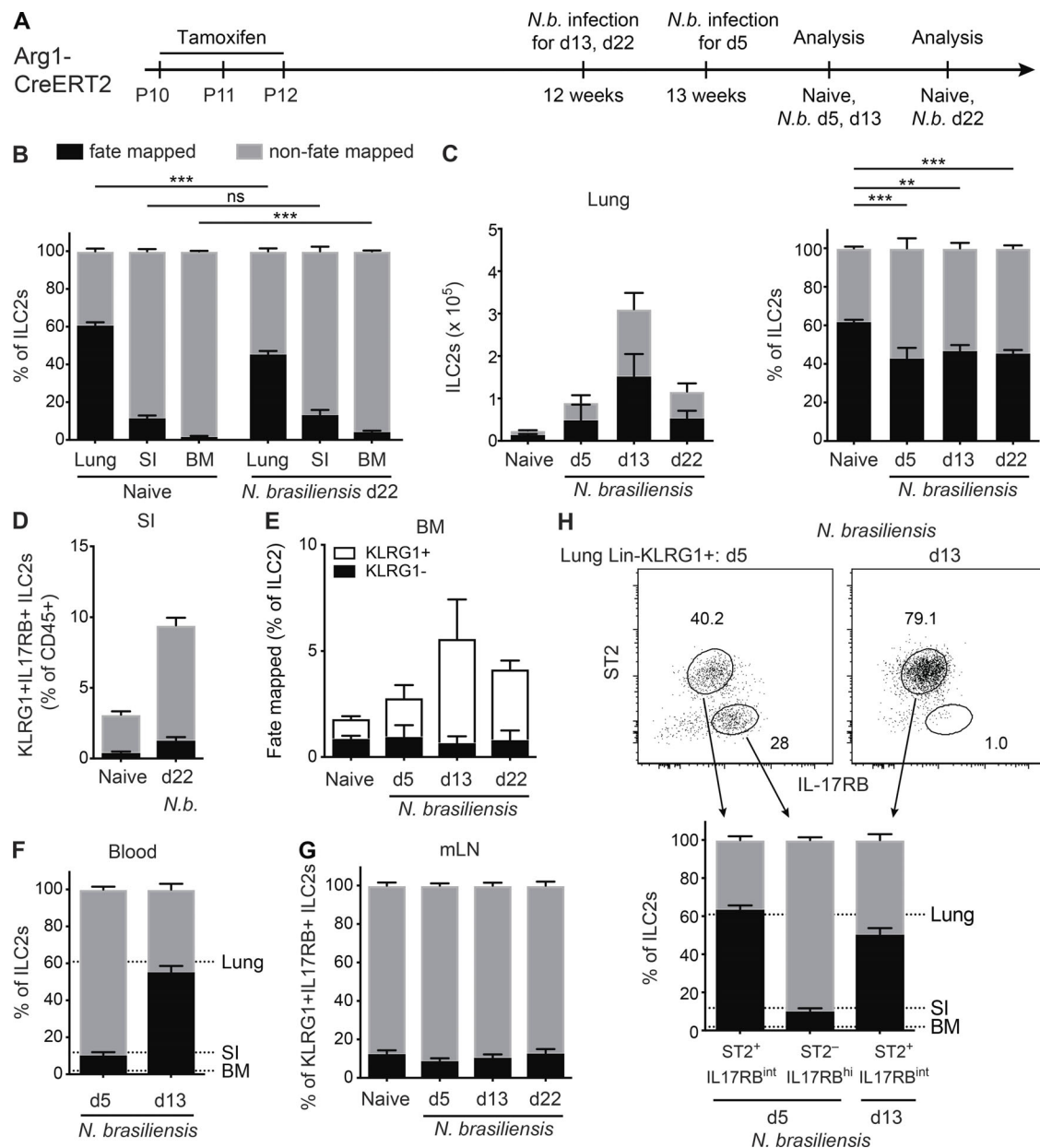
Figure 4. **Circulating ILC2s can be traced back to the tissue. (A–H)** *Arg1*[RFP-CreERT2]*R26R*[YFP] mice were tamoxifen treated on postnatal day (p)10, p11, and p12 according to the schedule in A. 10 wk later, mice were infected with *N. brasiliensis* (*N.b.*), and the ratios of fate-mapped and non–fate-mapped cells were analyzed on d5, d13, and d22 after infection. **(B)** Frequencies of fate-mapped (black bars) and non–fate-mapped (gray bars) ILC2s in the lung, small intestine lamina propria (SI), or BM from naive mice or d22 after infection with *N. brasiliensis*. **(C)** Total numbers (left) and frequencies (right) of fate-mapped ILC2s (CD45+Lin−KLRG1+IL-17RB+ and/or ST2+) in the lung d5, d13, or d22 after infection. **(D)** Frequencies of fate-mapped KLRG1+IL-17RB+ ILC2s from the small intestine. **(E)** Frequencies of fate-mapped KLRG1+ and KLRG1− ILC2s (CD45+Lin−IL-7Rα+ST2+Arg1-RFP+) in BM from naive mice on d5, d13, or d22 after infection. **(F)** Percentages of fate-mapped ILC2s (CD45+Lin−KLRG1+IL-17RB+ and/or ST2+) in the blood at d5 or d13 after infection. Dotted lines represent the mean frequency of fate-mapped percentage of ILC2s for indicated tissues of uninfected mice. **(G)** Frequencies of fate-mapped KLRG1+IL-17RB+ ILC2s from mLN. **(H)** Frequencies of fate-mapped cells among gated ILC2 subsets in the lung on d5 and d13. Data are from one experiment representative of at least two independent experiments displayed as mean ± SEM of four or five individual mice per group and time point. **, P < 0.005; ***, P < 0.0005. ns, no significant difference.

ILC2s in the intestine-draining mLN (Fig. 4 G). We also identified a population of IL-17RB+ST2− ILC2s in the d5 lung, which matched d5 blood and small intestine ILC2s in terms of surface marker expression and percentage of fate-mapped cells (Fig. 4 H), consistent with their small intestinal origin and dependence on IL-25 as proposed in prior studies (Fig. 3; Huang et al., 2015; Huang et al., 2018).

However, circulating ILC2s on d12 displayed threefold higher labeling frequencies, which matched their phenotypic counterparts in the lung (Fig. 4, F and H), consistent with derivation from activated pools of ILC2s in the lung rather than the small intestine and inconsistent with the alternative hypothesis of alterations in the surface phenotype of small intestine–derived ILC2s.

Distinct ILC2 subsets arise by niche extrusion during local tissue perturbation

Our results indicate that different waves of blood ILC2s are locally elicited due to the migratory life cycle of *N. brasiliensis*, which induces lung damage and potential IL-33 release while crossing the alveolar epithelial barrier (Marsland et al., 2008) and whose luminal presence in the small intestine after d3 acutely activates the IL-25–dependent tuft cell–ILC2 circuit (Gerbe et al., 2016; Howitt et al., 2016; von Moltke et al., 2016). Paradoxically, however, the blood ILC2 waves seem to originate first from the gut and only later from the lung. To establish this directly, we employed ways to restrict the larvae to either the lung or the small intestine (Harvie et al., 2010; Fig. 5 A). First, we treated mice with the anti-helminthic drug pyrantel pamoate in the drinking water from d1 to d12 after infection to kill the larvae, which enter the digestive tract after migrating from the lung. Oral pyrantel pamoate reduced the number of circulating ILC2s on d5, whereas the subsequent wave on d12 was comparable to that of untreated mice (Fig. 5, B and C). In contrast, bypassing the lung-damaging life cycle stages by oral gavage of mature adult worms resulted in the normal appearance of circulatory ILC2s on d5 but dramatically reduced the ILC2 wave on d12 (Fig. 5, B and C), indicating that perturbation of local tissue and generation of specific alarmins are critical for the activation of ILC2s. Indeed, oral gavage of adult worms prevented ILC2 expansion and activation of IL-13 expression in the lung on d12 (Fig. 5, D and E), as well as the local induction of IL-5^{+} T helper type 2 effector cells (Fig. 5, F and G), which was otherwise seen with s.c. infection of mice using L3 larvae or after blockade of the intestinal stage using pyrantel pamoate. However, bypassing the lung stage by oral gavage still led to the appearance of IL-17RB^{+}ST2^{−} ILC2s in the lung on d5 (Fig. 5 H). The gut-derived wave of ILC2s elicited by oral gavage had comparable capacity to produce IL-13 (Fig. 5 H). Furthermore, when bypassing the lung stage via oral gavage, the increase in serum IL-13 levels on d5 was still observed, corresponding to the extrusion of activated small intestine ILC2s, but reached undetectable levels by d12. (Fig. 5 I). In contrast, when the intestinal stage was blocked using pyrantel pamoate, the increase in levels of serum IL-13 was only detected on d12, when lung-derived ILC2s reached the circulation (Fig. 5 I). Overall, these results link the local presence of *N. brasiliensis* with activation-induced extrusion from tissue niches, resulting in temporally and phenotypically distinct waves of cytokine-secreting ILC2s in the circulating blood.

We showed that infection with the migratory helminth *N. brasiliensis* drives a robust and steady increase in circulatory ILC2s beginning on d5 after infection and continuing past the time of intestinal worm clearance, which occurs by d8–d9. Blood ILCs, consistent with a prior report (Huang et al., 2018), had an activated phenotype with evidence for recent division and active cytokine expression, as shown here using reporters and measurement of serum IL-13. Consistent with attenuation by FTY720, ILC2s entered the circulation from tissues and were CD69^{lo}. By using a combination of ILC2 cytokine receptor profiling (Ricardo-Gonzalez et al., 2018), fate-mapping, cytokine-deficient mice, and dissociation of the lung and intestinal phases of infection, we revealed unexpected temporal heterogeneity of

blood ILC2s in which small intestinal ILC2s first entered the blood and became replaced by a second wave of lung-derived ILC2s.

Huang et al. (2018) proposed that after infection with *N. brasiliensis*, the ILC2s present in the blood migrate to distant sites such as the lung and thereby adopt a lung-like phenotype. However, our fate-mapping data demonstrate that circulating ILC2s on d5 displayed receptor profiles and fate-mapping profiles that matched small intestine ILC2s while d12 ILC2s in the blood showed receptor profiles and fate-mapping profiles that matched their resident counterparts from the lung. Furthermore, based on the clear differences in fate-mapped cells, our results also demonstrate that a majority of expanded tissue ILC2 pools following helminth infection were not derived from BM ILC2s or their upstream progenitors, in agreement with previous reports (Gasteiger et al., 2015; Schneider et al., 2019). Thus, by d12, the majority of cells in the blood were not phenotypically converted ILC2s from the small intestine, but rather derived from activated pools of ILC2s in the lung. This interpretation is further supported by experiments involving concurrent administration of pyrantel pamoate or direct delivery of mature worms to the gastrointestinal tract by oral gavage. While oral gavage of worms generated the early (d5) "gut wave" of blood ILC2s comparable to natural infection, the secondary (d12) "lung wave" was substantially attenuated. Conversely, use of drugs after larval migration to the lung to curtail intestinal infection resulted in loss of the initial wave of blood ILC2s but preservation of the later wave. Further, the initial wave was almost completely abrogated in IL-25–deficient mice, whereas the second wave was abrogated in IL-33R–deficient mice, which correlates with the activating receptor profiles on tissue ILC2s in the small intestine and lung, respectively (Ricardo-Gonzalez et al., 2018).

The paradoxical appearance of blood ILC2s from distinct tissues in reverse order of the infectious cycle was unexpected. It is possible that in the small intestine, rapid release of IL-25 from activated tuft cells drives immediate proliferation of lamina propria ILC2s that egress from the tissue once the local niche capacity has been exceeded. Indeed, a recent report by Campbell et al. (2019) also showed that intestinal response to a variety of worm infections leads to IL-13–mediated effects in the lung and other mucosal sites in an S1PR-dependent manner. In the lung, tissue damage (Marsland et al., 2008), possibly in combination with inflammatory cell–derived endogenous proteases, is likely required to generate proteolytically activated IL-33 (Cayrol et al., 2018) that subsequently drives local proliferation and eventual extrusion of lung ILC2s into the circulation; this process may be further delayed by disruption of tissue architecture, perhaps accounting for the lesser effects of FTY720 on the second cytokine wave (Fig. 1 E). The molecular mechanisms of this process remain incompletely understood, but alterations in the ILC2 adventitial niches, which are proximal to the airways, may be involved (Dahlgren et al., 2019; Koga et al., 2018; Puttur et al., 2019).

Based on these findings, we propose that niche extrusion occurs when ILC2 population size exceeds the tissue carrying capacity as a consequence of temporally increased proliferative stimuli such as IL-25 and IL-33, perhaps in combination with
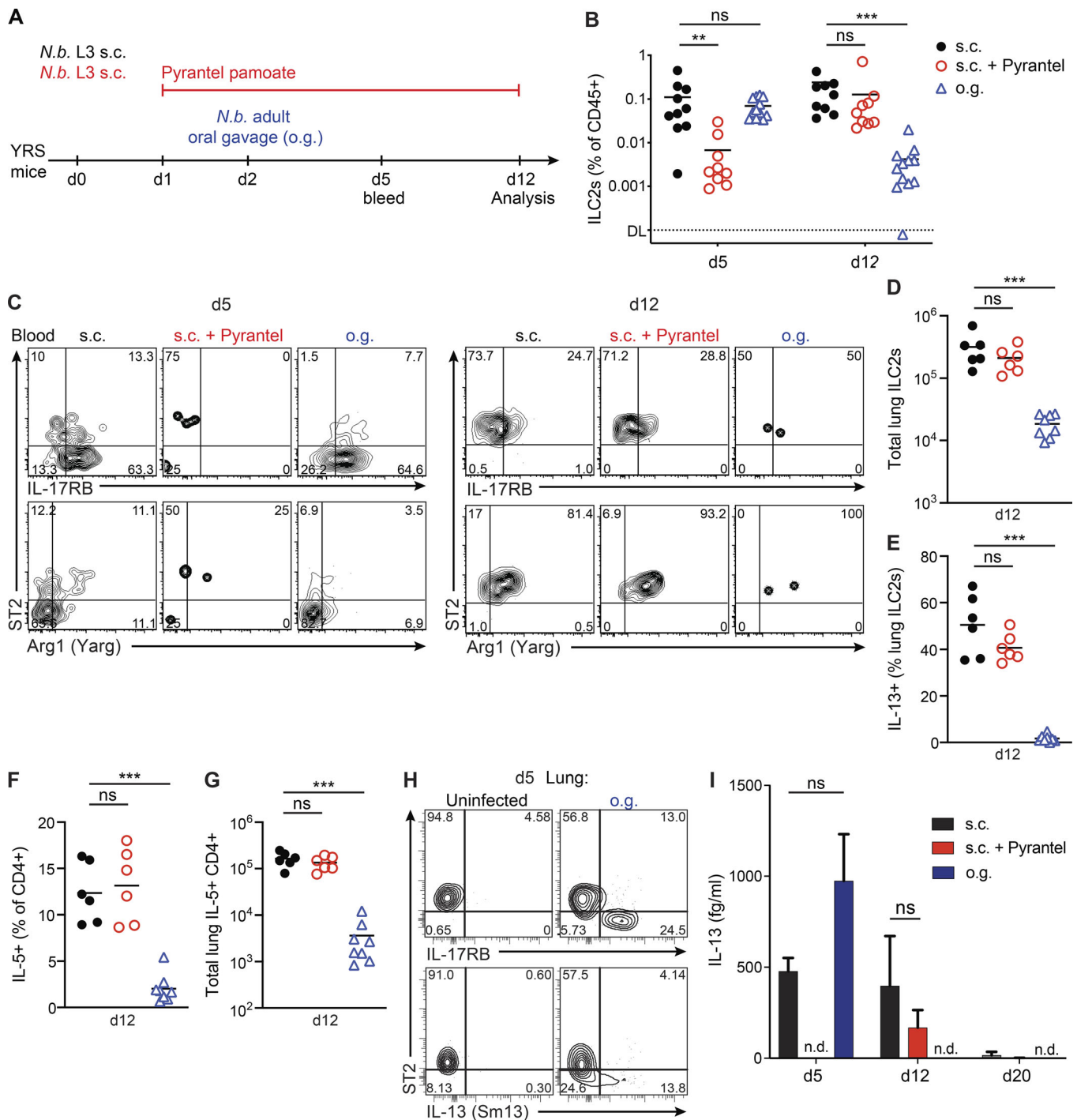
Ricardo-Gonzalez et al.
Niche extrusion of tissue ILC2s into circulation

Journal of Experimental Medicine   7 of 12
https://doi.org/10.1084/jem.20191172

Figure 5. Phenotypically distinct ILC2s arise by niche extrusion during local tissue perturbation. (A) Schematic of the infection protocol to isolate lung or small intestine exposure to *N. brasiliensis*. Groups of *Arg1*[Yarg]*Il5*[Red5]*Il13*[Sm13] (YRS) triple-reporter mice with individual treatments are color-coded. Black, standard s.c. infection (s.c.); red, s.c. infection followed by oral pyrantel pamoate treatment d1–d12 (s.c. + pyrantel); blue, oral gavage of adult *N. brasiliensis* worms (o.g.). Timeline relative to s.c. **(B)** Frequency of KLRG1^{+}IL-5 (Red5)[+] blood ILC2s. DL, detection limit. **(C)** Expression of ST2 and IL-17RB or Arg1 by IL-5^{+} cells gated on Lin^{−}CD45^{+} cells isolated from peripheral blood on d5 (left panels) and d12 (right panels). **(D and E)** Quantification of total IL-5^{+} ILC2s in the lung (D) and their expression of IL-13 (Sm13; E) analyzed on d12. **(F and G)** Frequency (F) or absolute number (G) of lung IL-5^{+} CD4^{+} T cells was analyzed on d12. **(H)** Expression of ST2 and IL-17RB (top panels) or ST2 and IL-13 (Sm13; bottom panels) by IL-5^{+} cells gated on Lin^{−}CD45^{+} cells isolated from d5 lung of naive (uninfected) or o.g. adult *N. brasiliensis*–infected mice as described in A. **(I)** Serum IL-13 levels from WT C57BL/6J mice infected with *N. brasiliensis* as described in A and displayed as mean ± SEM. n.d., not detected. Data are pooled from two independent experiments and 9–12 individual mice per group (B) or from one experiment representative of two independent experiments (C–I). **, $P < 0.005$; ***, $P < 0.0005$. ns, no significant difference; *N.b.*, *N. brasiliensis*.

additional activating ligands from neurons or other tissues (Klose and Artis, 2019). The concept of carrying capacity was recently applied to macrophage–fibroblast growth factor exchange circuits and supported by computational methods and experimental approaches in vitro (Zhou et al., 2018), although whether regulation of immune cell population size in vivo occurs through cell death or displacement is unclear. Our results suggest that niche extrusion may be a mechanism whereby ILC2 population size is regulated to fit niche size. Notably, carrying capacity does not have to be static, but may be dynamically affected by niche remodeling, as indicated by increased ILC2s in the lung that persisted many weeks after tissue perturbation (Martinez-Gonzalez et al., 2016; Van Dyken et al., 2016).

Although expansion of tissue ILC2 populations following tissue perturbation occurs locally, as shown here and previously (Gasteiger et al., 2015; Schneider et al., 2019), with minimal contribution from ILC precursors residing in the BM (Klose et al., 2014; Walker et al., 2019; Xu et al., 2019) or present in the circulation (Bar-Ephraim et al., 2019; Lim et al., 2017), niche extrusion disseminates ILC2s such that type 2 cytokines appear in the blood accordingly. As such, an otherwise localized response becomes systemically distributed, akin to hormonal responses that operate at distant sites. We cannot exclude the possibility that a subset of ILC(2) progenitors in the BM or elsewhere retains the labeling at a frequency that is similar to that of ILC2s in the lung or small intestine; in addition, these studies did not address the long-term capacity of these cells to adjust to altered tissue environments (Huang et al., 2018). More sophisticated tissue-specific marking tools for ILC2s are necessary to determine the ultimate fate and disposition of these cells under various inflammatory and allergic settings, but the relatively rapid disappearance of activated ILC2s after the conclusion of *N. brasiliensis* infection suggests this period is regulated. Further study is needed to address whether the concept of niche extrusion applies to other tissue lymphocyte populations, including tissue-resident memory T cells, which share properties of residency and turnover with ILCs (Masopust and Soerens, 2019). Indeed, some of these tissue-resident memory T cells may redistribute and position in secondary lymphoid organs upon antigen reexposure (Beura et al., 2018), and transfer experiments suggest that reactivated resident memory T cells give rise to cells that enter the systemic circulation (Masopust et al., 2006), potentially facilitating the systemic dissemination of cytokines as shown here.

Materials and methods
Mice
Arg1[Yarg] (Yarg; B6.129S4-*Arg1*[tm1Lky]/J; 015857; Reese et al., 2007), *Il5*[Red5] (Red5; B6[C]-*Il5*[tm1.1(icre)Lky]/J; 030926; Nussbaum et al., 2013), *Il13*[Smart] (Smart13; B6.129S4[C]-*Il13*[tm2.1Lky]/J; 031367; Liang et al., 2011), and *Arg1*[RFP-CreERT2] (Schneider et al., 2019) mice have been previously described. *R26R*[YFP] (B6.129X1-*Gt[ROSA]26Sor*[tm1[EYFP]Cos]/J; 006148) and WT (C57BL/6J; 000664) mice were purchased from the Jackson Laboratory. B6.*Il25*^{−/−} and B6.*Il1rl1*^{−/−} mice were obtained and crossed to the *Il5*[Red5], *Arg1*[Yarg], and *Il13*[Smart] reporter mice as previously described (Ricardo-Gonzalez et al., 2018).

All mice were generated on or backcrossed to the C57BL/6 background. Mice were maintained in the University of California, San Francisco (UCSF) specific pathogen–free animal facility in accordance with the guidelines established by the Institutional Animal Care and Use Committee and Laboratory Animal Resource Center. SPF animals were housed in individually ventilated cage units that were changed every 3 wk for maintenance cages and every other week for breeding cages; cage bottoms were covered with autoclaved bedding and nesting material for enrichment. Mice were fed irradiated food (PicoLab Mouse Diet 20, 5058M) and drank from autoclaved bottles or an automatic watering system. All animals were manipulated using standard procedures, including filtered air exchange stations and chlorine-based disinfection of gloves and work surfaces within manipulations with animals; personnel protection equipment (disposable gowns, gloves, head caps, and shoe covers) was required before entering the facility. Experiments were performed using age- and gender-matched groups. All animal procedures were approved by the UCSF Institutional Animal Care and Use Committee.

Tissue dissociation
Mice were bled at indicated time points as noted in the figures. Mouse whole blood was washed with cold PBS supplemented with 5 mM EDTA pH 8.0 (Teknova). Red blood cell lysing was performed using Pharm Lyse lysing buffer (BD Biosciences) before antibody staining. Mouse lungs were perfused through the right cardiac ventricle with cold PBS and underwent an initial mechanical dissociation using the m_lung_01_01 program on the gentleMACS Dissociator (Miltenyi Biotec). Lung tissues were then digested with 50 µg/ml Liberase TM (Roche) and 25 µg/ml DNase I (Roche) in prewarmed RPMI-1640 for 30 min at 37°C. Further dissociation was performed using the m_lung_01_02 program on the gentleMACS Dissociator. Single-cell suspensions were obtained after passing the homogenized samples through 70-µm cell strainers.

Mouse intestines were flushed with PBS, and Peyer's patches were removed when visible in older mice. Intestines were opened, thoroughly cleaned with PBS, and incubated for 20 min in 20 ml HBSS (Ca^{2+}/Mg^{2+} free) supplemented with 2% FCS, 10 mM Hepes (UCSF Cell Culture Facility), and 5 mM dithiothreitol. Supernatants were discarded, and intestines were incubated for 15 min in 10 ml HBSS (Ca^{2+}/Mg^{2+} free) supplemented with 2% FCS, 10 mM Hepes (UCSF Cell Culture Facility), and 5 mM EDTA solution. This step was repeated twice using fresh solution. Next, intestines were incubated for 10 min in 20 ml HBSS (with Ca^{2+}/Mg^{2+}) supplemented with 3% FCS and 10 mM Hepes. After incubation, intestines were gently vortexed, cut into small pieces, and incubated for 30 min in 5 ml HBSS (with Ca^{2+}/Mg^{2+}) supplemented with 3% FCS, 10 mM Hepes, 100 µg/ml Liberase TM, and 30 µg/ml DNase I. All incubations were performed with gentle rocking at 37°C. After digest, intestines were mechanically dissociated in GentleMACS C tubes (Miltenyi Biotec) using program m_intestine_01, passed through a 100-µm filter, and washed. The resulting cell pellet was resuspended in 5 ml 40% Percoll (Sigma-Aldrich), underlaid with 5 ml 90% Percoll, and centrifuged at 2,000 rpm for 20 min at 20°C. The

Ricardo-Gonzalez et al.
Niche extrusion of tissue ILC2s into circulation

Journal of Experimental Medicine
https://doi.org/10.1084/jem.20191172

9 of 12

40/90 interphase of the Percoll gradient was harvested, washed, and stained for flow cytometry.

mLNs were gently dissociated over a 70-μm nylon filter using a syringe plunger and washed with PBS with 3% FCS.

Flow cytometry

Fc block (anti-mouse CD16/32, 2.4G2) was purchased from Bio-XCell. Rat anti-mouse CD4 (RM4-5), rat anti-mouse CD11b (M1/70), rat anti-mouse CD19 (ID3), and rat anti-mouse B220 (RB6-8C5) were purchased from BD Pharmingen; rat anti-mouse c-kit (2B8), rat anti-mouse CD3 (17A2), rat anti-mouse CD5 (53–7.3), rat anti-mouse CD127 (A7R34), rat anti-mouse NKp46 (29A1.4), mouse anti-mouse CD45.2 (104), rat anti-human/mouse GATA-3 (TWAJ), rat anti-mouse Ki67 (SolA15), and mouse anti-mouse NK1.1 (PK136) antibodies were purchased from eBioscience; Armenian hamster anti-mouse CD11c (N418), Syrian hamster anti-mouse KLRG1 (2F1), rat anti-mouse CD45 (30-F11), rat anti-mouse Ter119 (TER-119), rat anti-mouse CD25 (PC61), rat anti-mouse IL-17RB (9B10), rat anti-mouse CD90.2 (30-H12), and rat anti-mouse F4/80 (BM8) antibodies were purchased from BioLegend; and rat anti-mouse ST2 (DJ8) antibodies were purchased from MD Bioproducts. Lin$^-$ cells were defined as lacking CD3, CD4, CD5, CD8α, CD11b, CD11c, CD19, NK1.1, F4/80, Gr-1, FcεRIα, and Ter119. DAPI and Live/Dead (Invitrogen) were used for dead-cell exclusion for live and fixed samples, respectively. For intracellular staining of transcription factors, the FoxP3/Transcription Factor Staining Buffer Set (eBioscience) was used according to manufacturer's instructions.

Samples were analyzed on an LSRFortessa X20 (BD Biosciences) with five lasers (355 nm, 405 nm, 488 nm, 561 nm, and 640 nm). Samples were gated by FSC-A/SSC-A to exclude debris, FSC-H/FSC-W for single cells, and gated to exclude dead cells by DAPI (unfixed samples) or Live/Dead (fixed samples). Data analysis was performed using FlowJo (Treestar).

N. brasiliensis infection and treatments

For infections with *N. brasiliensis*, mice were injected s.c. with 500 L3 stage larvae and analyzed at the indicated time points after infection. For oral gavage of *N. brasiliensis*, rats were infected and adult worms were harvested from the small intestine 7 d after infection. 500 adult worms were then administered by oral gavage 2 d later than the standard L3 s.c. injection to mimic the intestinal stage of the infectious cycle. To prevent *N. brasiliensis* from finishing the life cycle in the small intestine, mice were injected s.c. with 500 L3 stage larvae and treated with 5 mg/ml pyrantel pamoate (Columbia Laboratories) in the drinking water starting at 24–30 h after infection until analysis.

Tamoxifen treatments

Tamoxifen was dissolved at 40 mg/ml in 100% ethanol and supplemented with one volume of Cremophor EL (Sigma-Aldrich;C5135), and aliquots were stored at –80°C. After thawing in a thermomixer, two volumes of PBS was added for a final concentration of 10 mg/ml tamoxifen. Neonatal pups were injected i.p. with 400 μg tamoxifen on postnatal d10, d11, and d12.

Cytokine quantification

Cytokine levels in mouse serum were measured using Cytokine Bead Array Flex Sets (BD Biosciences) according to the manufacturer's protocol, and data were analyzed using Flow Cytometric Analysis Program Array software (BD Biosciences).

CD45 antibody injection

Mice were anesthetized and injected with 3 μg of mouse anti-mouse APC-Cy7-CD45.2 (eBioscience; clone 104) antibody via cardiac injection. Mice were sacrificed 3 min later, and tissues were processed as described above.

FTY720 treatment

Mice were infected with *N. brasiliensis* as indicated above. FTY720 (Tocris) was dissolved in normal saline. Mice were treated daily with 1 mg/kg FTY720 i.p. or alternatively with normal saline starting on the day of infection and sacrificed at the time points indicated in the figures.

Statistical analysis

All experiments were performed using randomly assigned mice without investigator blinding. All data points and n values reflect biological replicates. No data were excluded. Where noted in the figures, statistical significance was calculated using the two-tailed nonparametric Mann-Whitney U test or the unpaired two-tailed t test for comparison between two experimental groups or one-way ANOVA for multiple comparisons. Experimental groups included a minimum of three biological replicates. Intragroup variation was not assessed. All statistical analysis was performed using Prism 8 (GraphPad Software). Figures display means ± SEM as indicated. No statistical methods were used to predetermine sample size.

Online supplemental material

Fig. S1 shows the ILC2 gating strategy for experiments using *Arg1*^{Yarg}*Il5*^{Red5}*Il13*^{Sm13} (YRS) triple-reporter or C57BL/6J mice. Fig. S2 shows effector cytokine production and proliferation of ILC2s after *N. brasiliensis* infection and treatment with FTY720 and their labeling following i.v. injection of anti-CD45 antibody. Fig. S3 shows the expression of *Arg1*-RFP-CreERT2;*R26*-YFP reporter by *Id2*-GFP$^+$Lin$^-$ BM cells and the gating strategy to identify blood ILC2s in fate-mapping experiments.

References

Bar-Ephraim, Y.E., J.J. Koning, E. Burniol Ruiz, T. Konijn, V.P. Mourits, K.A. Lakeman, L. Boon, M. Bögels, J.P. van Maanen, J.M.M. Den Haan, et al. 2019. CD62L Is a Functional and Phenotypic Marker for Circulating Innate Lymphoid Cell Precursors. *J. Immunol.* 202:171–182. https://doi.org/10.4049/jimmunol.1701153

Beura, L.K., S. Wijeyesinghe, E.A. Thompson, M.G. Macchietto, P.C. Rosato, M.J. Pierson, J.M. Schenkel, J.S. Mitchell, V. Vezys, B.T. Fife, et al. 2018. T Cells in Nonlymphoid Tissues Give Rise to Lymph-Node-Resident Memory T Cells. *Immunity.* 48:327–338.e5. https://doi.org/10.1016/j.immuni.2018.01.015

Bouchery, T., B. Volpe, K. Shah, L. Lebon, K. Filbey, G. LeGros, and N. Harris. 2017. The Study of Host Immune Responses Elicited by the Model Murine Hookworms Nippostrongylus brasiliensis and Heligmosomoides polygyrus. *Curr. Protoc. Mouse Biol.* 7:236–286. https://doi.org/10.1002/cpmo.34

Campbell, L., M.R. Hepworth, J. Whittingham-Dowd, S. Thompson, A.J. Bancroft, K.S. Hayes, T.N. Shaw, B.F. Dickey, A.L. Flamar, D. Artis, et al. 2019. ILC2s mediate systemic innate protection by priming mucus production at distal mucosal sites. *J. Exp. Med.* 216:2714–2723. https://doi.org/10.1084/jem.20180610

Cayrol, C., A. Duval, P. Schmitt, S. Roga, M. Camus, A. Stella, O. Burlet-Schiltz, A. Gonzalez-de-Peredo, and J.P. Girard. 2018. Environmental allergens induce allergic inflammation through proteolytic maturation of IL-33. *Nat. Immunol.* 19:375–385. https://doi.org/10.1038/s41590-018-0067-5

Cherrier, D.E., N. Serafini, and J.P. Di Santo. 2018. Innate Lymphoid Cell Development: A T Cell Perspective. *Immunity.* 48:1091–1103. https://doi.org/10.1016/j.immuni.2018.05.010

Dahlgren, M.W., S.W. Jones, K.M. Cautivo, A. Dubinin, J.F. Ortiz-Carpena, S. Farhat, K.S. Yu, K. Lee, C. Wang, A.V. Molofsky, et al. 2019. Adventitial Stromal Cells Define Group 2 Innate Lymphoid Cell Tissue Niches. *Immunity.* 50:707–722.e6. https://doi.org/10.1016/j.immuni.2019.02.002

Gasteiger, G., X. Fan, S. Dikiy, S.Y. Lee, and A.Y. Rudensky. 2015. Tissue residency of innate lymphoid cells in lymphoid and nonlymphoid organs. *Science.* 350:981–985. https://doi.org/10.1126/science.aac9593

Gerbe, F., E. Sidot, D.J. Smyth, M. Ohmoto, I. Matsumoto, V. Dardalhon, P. Cesses, L. Garnier, M. Pouzolles, B. Brulin, et al. 2016. Intestinal epithelial tuft cells initiate type 2 mucosal immunity to helminth parasites. *Nature.* 529:226–230. https://doi.org/10.1038/nature16527

Ghaedi, M., C.A. Steer, I. Martinez-Gonzalez, T.Y.F. Halim, N. Abraham, and F. Takei. 2016. Common-Lymphoid-Progenitor-Independent Pathways of Innate and T Lymphocyte Development. *Cell Reports.* 15:471–480. https://doi.org/10.1016/j.celrep.2016.03.039

Harvie, M., M. Camberis, S.C. Tang, B. Delahunt, W. Paul, and G. Le Gros. 2010. The lung is an important site for priming CD4 T-cell-mediated protective immunity against gastrointestinal helminth parasites. *Infect. Immun.* 78:3753–3762. https://doi.org/10.1128/IAI.00502-09

Howitt, M.R., S. Lavoie, M. Michaud, A.M. Blum, S.V. Tran, J.V. Weinstock, C.A. Gallini, K. Redding, R.F. Margolskee, L.C. Osborne, et al. 2016. Tuft cells, taste-chemosensory cells, orchestrate parasite type 2 immunity in the gut. *Science.* 351:1329–1333. https://doi.org/10.1126/science.aaf1648

Huang, Y., L. Guo, J. Qiu, X. Chen, J. Hu-Li, U. Siebenlist, P.R. Williamson, J.F. Urban Jr., and W.E. Paul. 2015. IL-25-responsive, lineage-negative KLRG1(hi) cells are multipotential 'inflammatory' type 2 innate lymphoid cells. *Nat. Immunol.* 16:161–169. https://doi.org/10.1038/ni.3078

Huang, Y., K. Mao, X. Chen, M.A. Sun, T. Kawabe, W. Li, N. Usher, J. Zhu, J.F. Urban Jr., W.E. Paul, and R.N. Germain. 2018. S1P-dependent interorgan trafficking of group 2 innate lymphoid cells supports host defense. *Science.* 359:114–119. https://doi.org/10.1126/science.aam5809

Karta, M.R., P.S. Rosenthal, A. Beppu, C.Y. Vuong, M. Miller, S. Das, R.C. Kurten, T.A. Doherty, and D.H. Broide. 2018. β2 integrins rather than β1 integrins mediate Alternaria-induced group 2 innate lymphoid cell trafficking to the lung. *J. Allergy Clin. Immunol.* 141:329–338.e12. https://doi.org/10.1016/j.jaci.2017.03.010

Klose, C.S., and D. Artis. 2019. Neuronal regulation of innate lymphoid cells. *Curr. Opin. Immunol.* 56:94–99. https://doi.org/10.1016/j.coi.2018.11.002

Klose, C.S.N., M. Flach, L. Möhle, L. Rogell, T. Hoyler, K. Ebert, C. Fabiunke, D. Pfeifer, V. Sexl, D. Fonseca-Pereira, et al. 2014. Differentiation of type 1 ILCs from a common progenitor to all helper-like innate lymphoid cell lineages. *Cell.* 157:340–356. https://doi.org/10.1016/j.cell.2014.03.030

Koga, S., K. Hozumi, K.I. Hirano, M. Yazawa, T. Terooatea, A. Minoda, T. Nagasawa, S. Koyasu, and K. Moro. 2018. Peripheral PDGFRα+gp38+ mesenchymal cells support the differentiation of fetal liver-derived ILC2. *J. Exp. Med.* 215:1609–1626. https://doi.org/10.1084/jem.20172310

Kotas, M.E., and R.M. Locksley. 2018. Why Innate Lymphoid Cells? *Immunity.* 48:1081–1090. https://doi.org/10.1016/j.immuni.2018.06.002

Liang, H.-E., R.L. Reinhardt, J.K. Bando, B.M. Sullivan, I.C. Ho, and R.M. Locksley. 2011. Divergent expression patterns of IL-4 and IL-13 define unique functions in allergic immunity. *Nat. Immunol.* 13:58–66. https://doi.org/10.1038/ni.2182

Lim, A.I., Y. Li, S. Lopez-Lastra, R. Stadhouders, F. Paul, A. Casrouge, N. Serafini, A. Puel, J. Bustamante, L. Surace, et al. 2017. Systemic Human ILC Precursors Provide a Substrate for Tissue ILC Differentiation. *Cell.* 168:1086–1100.e10: E10. https://doi.org/10.1016/j.cell.2017.02.021

Marsland, B.J., M. Kurrer, R. Reissmann, N.L. Harris, and M. Kopf. 2008. Nippostrongylus brasiliensis infection leads to the development of emphysema associated with the induction of alternatively activated macrophages. *Eur. J. Immunol.* 38:479–488. https://doi.org/10.1002/eji.200737827

Martinez-Gonzalez, I., L. Mathä, C.A. Steer, M. Ghaedi, G.F. Poon, and F. Takei. 2016. Allergen-Experienced Group 2 Innate Lymphoid Cells Acquire Memory-like Properties and Enhance Allergic Lung Inflammation. *Immunity.* 45:198–208. https://doi.org/10.1016/j.immuni.2016.06.017

Masopust, D., and A.G. Soerens. 2019. Tissue-Resident T Cells and Other Resident Leukocytes. *Annu. Rev. Immunol.* 37:521–546. https://doi.org/10.1146/annurev-immunol-042617-053214

Masopust, D., V. Vezys, E.J. Wherry, D.L. Barber, and R. Ahmed. 2006. Cutting edge: gut microenvironment promotes differentiation of a unique memory CD8 T cell population. *J. Immunol.* 176:2079–2083. https://doi.org/10.4049/jimmunol.176.4.2079

Moro, K., H. Kabata, M. Tanabe, S. Koga, N. Takeno, M. Mochizuki, K. Fukunaga, K. Asano, T. Betsuyaku, and S. Koyasu. 2016. Interferon and IL-27 antagonize the function of group 2 innate lymphoid cells and type 2 innate immune responses. *Nat. Immunol.* 17:76–86. https://doi.org/10.1038/ni.3309

Neill, D.R., S.H. Wong, A. Bellosi, R.J. Flynn, M. Daly, T.K.A. Langford, C. Bucks, C.M. Kane, P.G. Fallon, R. Pannell, et al. 2010. Nuocytes represent a new innate effector leukocyte that mediates type-2 immunity. *Nature.* 464:1367–1370. https://doi.org/10.1038/nature08900

Nussbaum, J.C., S.J. Van Dyken, J. von Moltke, L.E. Cheng, A. Mohapatra, A.B. Molofsky, E.E. Thornton, M.F. Krummel, A. Chawla, H.-E. Liang, and R.M. Locksley. 2013. Type 2 innate lymphoid cells control eosinophil homeostasis. *Nature.* 502:245–248. https://doi.org/10.1038/nature12526

Puttur, F., L. Denney, L.G. Gregory, J. Vuononvirta, R. Oliver, L.J. Entwistle, S.A. Walker, M.B. Headley, E.J. McGhee, J.E. Pease, et al. 2019. Pulmonary environmental cues drive group 2 innate lymphoid cell dynamics in mice and humans. *Sci. Immunol.* 4:eaav7638. https://doi.org/10.1126/sciimmunol.aav7638

Reese, T.A., H.-E. Liang, A.M. Tager, A.D. Luster, N. Van Rooijen, D. Voehringer, and R.M. Locksley. 2007. Chitin induces accumulation in tissue of innate immune cells associated with allergy. *Nature.* 447:92–96. https://doi.org/10.1038/nature05746

Ricardo-Gonzalez, R.R., S.J. Van Dyken, C. Schneider, J. Lee, J.C. Nussbaum, H.E. Liang, D. Vaka, W.L. Eckalbar, A.B. Molofsky, D.J. Erle, and R.M.

Locksley. 2018. Tissue signals imprint ILC2 identity with anticipatory function. *Nat. Immunol.* 19:1093–1099. https://doi.org/10.1038/s41590 -018-0201-4

Schneider, C., C.E. O'Leary, J. von Moltke, H.E. Liang, Q.Y. Ang, P.J. Turnbaugh, S. Radhakrishnan, M. Pellizzon, A. Ma, and R.M. Locksley. 2018. A Metabolite-Triggered Tuft Cell-ILC2 Circuit Drives Small Intestinal Remodeling. *Cell.* 174:271–284.e14. https://doi.org/10.1016/j.cell.2018.05 .014

Schneider, C., J. Lee, S. Koga, R.R. Ricardo-Gonzalez, J.C. Nussbaum, L.K. Smith, S.A. Villeda, H.E. Liang, and R.M. Locksley. 2019. Tissue-Resident Group 2 Innate Lymphoid Cells Differentiate by Layered Ontogeny and In Situ Perinatal Priming. *Immunity.* 50:1425–1438.e5. https://doi.org/10.1016/j.immuni.2019.04.019

Stier, M.T., J. Zhang, K. Goleniewska, J.Y. Cephus, M. Rusznak, L. Wu, L. Van Kaer, B. Zhou, D.C. Newcomb, and R.S. Peebles Jr. 2018. IL-33 promotes the egress of group 2 innate lymphoid cells from the bone marrow. *J. Exp. Med.* 215:263–281. https://doi.org/10.1084/jem.20170449

Van Dyken, S.J., J.C. Nussbaum, J. Lee, A.B. Molofsky, H.E. Liang, J.L. Pollack, R.E. Gate, G.E. Haliburton, C.J. Ye, A. Marson, et al. 2016. A tissue checkpoint regulates type 2 immunity. *Nat. Immunol.* 17:1381–1387. https://doi.org/10.1038/ni.3582

Vély, F., V. Barlogis, B. Vallentin, B. Neven, C. Piperoglou, M. Ebbo, T. Perchet, M. Petit, N. Yessaad, F. Touzot, et al. 2016. Evidence of innate lymphoid cell redundancy in humans. *Nat. Immunol.* 17:1291–1299. https://doi.org/10.1038/ni.3553

Vivier, E., D. Artis, M. Colonna, A. Diefenbach, J.P. Di Santo, G. Eberl, S. Koyasu, R.M. Locksley, A.N.J. McKenzie, R.E. Mebius, et al. 2018. Innate Lymphoid Cells: 10 Years On. *Cell.* 174:1054–1066. https://doi.org/10 .1016/j.cell.2018.07.017

von Moltke, J., M. Ji, H.E. Liang, and R.M. Locksley. 2016. Tuft-cell-derived IL-25 regulates an intestinal ILC2-epithelial response circuit. *Nature.* 529:221–225. https://doi.org/10.1038/nature16161

Walker, J.A., P.A. Clark, A. Crisp, J.L. Barlow, A. Szeto, A.C.F. Ferreira, B.M.J. Rana, H.E. Jolin, N. Rodriguez-Rodriguez, M. Sivasubramaniam, et al. 2019. Polychromic Reporter Mice Reveal Unappreciated Innate Lymphoid Cell Progenitor Heterogeneity and Elusive ILC3 Progenitors in Bone Marrow. *Immunity.* 51:104–118.e7. https://doi.org/10.1016/j .immuni.2019.05.002

Xu, W., D.E. Cherrier, S. Chea, C. Vosshenrich, N. Serafini, M. Petit, P. Liu, R. Golub, and J.P. Di Santo. 2019. An Id2[RFP]-Reporter Mouse Redefines Innate Lymphoid Cell Precursor Potentials. *Immunity.* 50:1054–1068.e3. https://doi.org/10.1016/j.immuni.2019.02.022

Zhou, X., R.A. Franklin, M. Adler, J.B. Jacox, W. Bailis, J.A. Shyer, R.A. Flavell, A. Mayo, U. Alon, and R. Medzhitov. 2018. Circuit Design Features of a Stable Two-Cell System. *Cell.* 172:744–757.e17. https://doi.org/10.1016/j .cell.2018.01.015
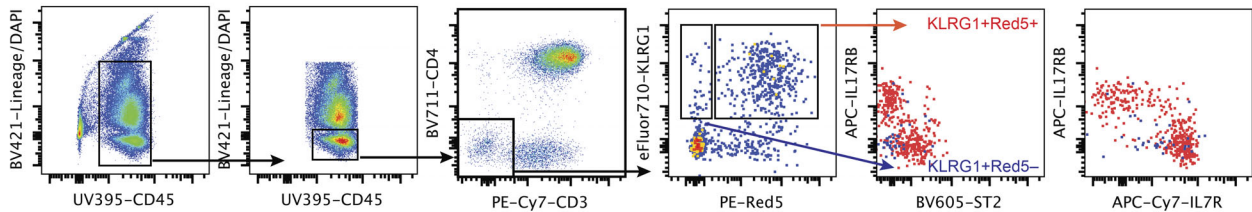
Supplemental material

A
Gating for experiments using *Il5*^{Red5} reporter mice
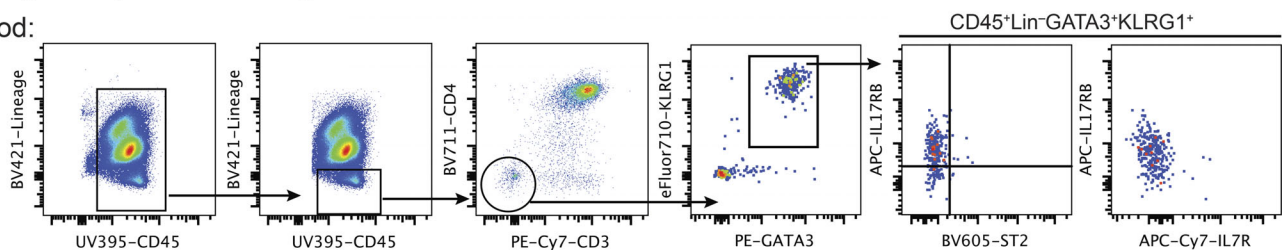
Blood:
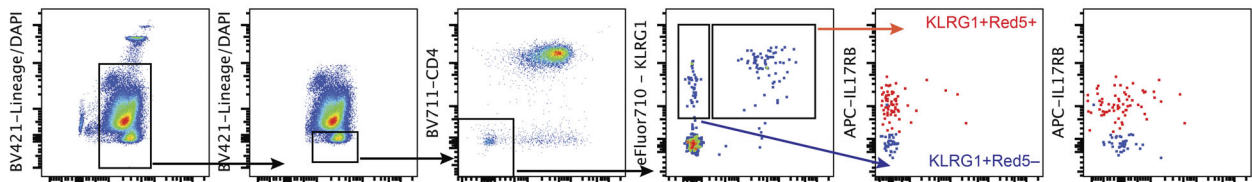
Lung:

B
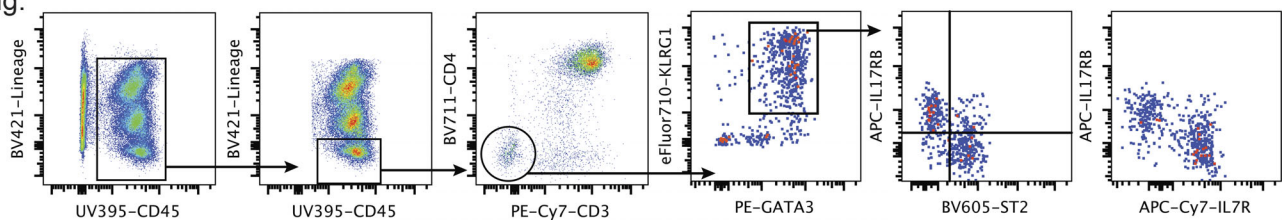Gating for experiments using C57BL/6J mice

Blood:

Lung:

Figure S1. **ILC2 gating strategy for experiments using reporter and B6 WT mice. (A and B)** Gating strategy for experiments using *Arg1*^{Yarg}*Il5*^{Red5}*Il13*^{Sm13} (YRS) triple-reporter mice (A) or C57BL/6J mice (B). Data are representative plots for the indicated organs at d5 after *N. brasiliensis*. Data shown are representative of more than three independent experiments with *n* ≥ 3 individual mice per group. PE, phycoerythrin.
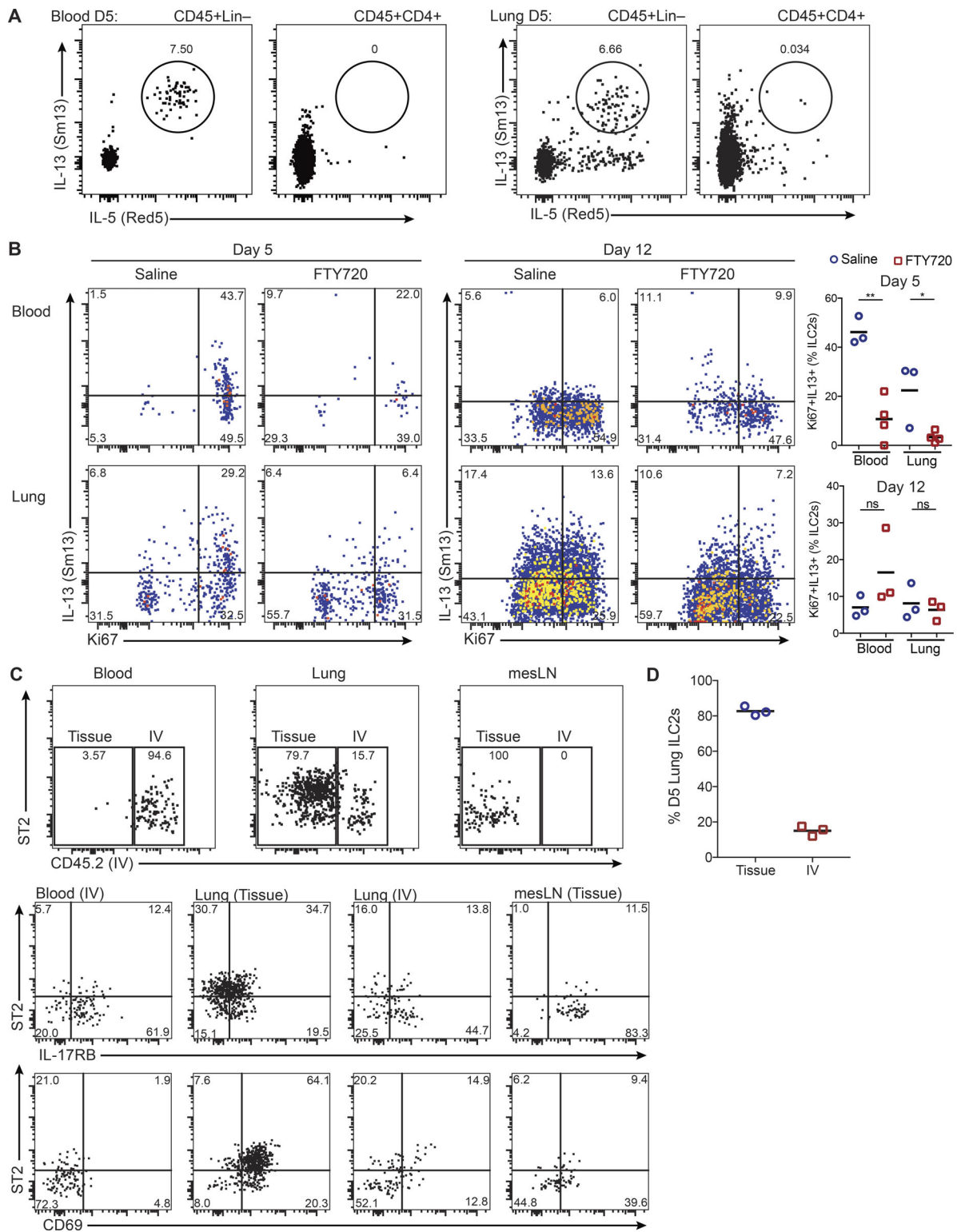
Ricardo-Gonzalez et al.
Niche extrusion of tissue ILC2s into circulation

Journal of Experimental Medicine   S1
https://doi.org/10.1084/jem.20191172

Figure S2. **Circulating ILC2s phenotypically differ during the course of *N. brasiliensis* infection. (A)** *Arg1*[Yarg]*Il5*[Red5]*Il13*[Sm13] (YRS) triple-reporter mice were infected with *N. brasiliensis,* and blood (left panels) and lungs (right panels) were analyzed on d5 after infection for IL-5 (Red5) and IL-13 (Sm13) expression in ILCs (gated on CD45+Lin−) and CD4 T cells (gated on CD45+CD4+). **(B)** Mice were infected with *N. brasiliensis* in the presence or absence of FTY720 (1 mg/kg), and blood (top panels) and lung (bottom panels) ILC2s (gated on CD45+Lin−GATA3+) were examined on d5 or d12 for IL-13 (Sm13) expression and Ki-67 labeling. **(C and D)** Mice were infected with *N. brasiliensis* and were i.v. injected with 3 µg of APC-Cy7–labeled CD45.2 antibody on d5 and euthanized 3 min later. **(C)** Top panels indicate the intravascular (IV) or tissue-resident (Tissue) ILC2s gated on CD45+Lin−IL5 (Red5)+ from the blood, lung, or mLNs (mesLN). Middle and bottom panels show the expression of ST2 and IL-17RB (middle panels) or ST2 and CD69 (bottom panels) from the intravascular or tissue-resident fraction from tissues as indicated. **(D)** Percentage of tissue and blood (IV) ILC2s in the lung on d5. Data are from one experiment representative of at least two independent experiments. *, P < 0.05; **, P < 0.005. ns, no significant difference.
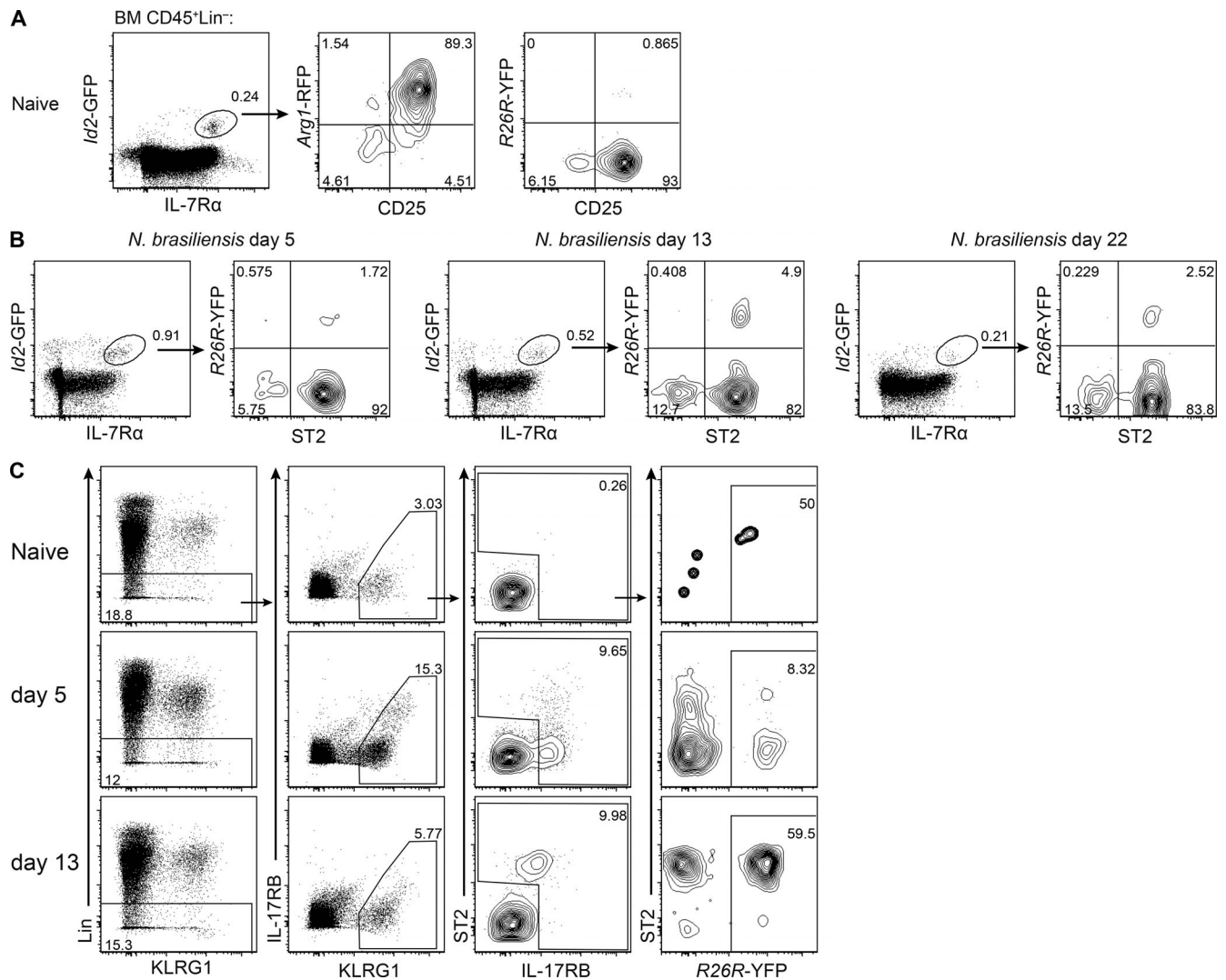
Figure S3.   **Circulating ILC2s can be traced back to the tissue. (A–C)** Mice were tamoxifen treated on p10, p11, and p12 as in Fig. 4. 10 wk later, mice were analyzed naive or after infection with *N. brasiliensis* at the indicated time points. **(A)** Expression of CD25 and *Arg1*-RFP or *R26R*-YFP by *Id2*-GFP+IL-7Rα+ cells gated on CD45+Lin− cells isolated from the BM of naive *Id2*GFP*Arg1*RFP-CreERT2*R26R*YFP reporter mice. **(B)** Expression of ST2 and *R26R*-YFP by *Id2*-GFP+IL-7Rα+ cells gated on CD45+Lin− cells isolated from the BM of *Id2*GFP*Arg1*RFP-CreERT2*R26R*YFP reporter mice on d5, d13, and d22 after infection with *N. brasiliensis*. **(C)** Gating strategy that was used to determine the fate-mapping frequency in ILC2s (CD45+Lin−KLRG1+IL-17RB+ and/or ST2+) from the blood of *Arg1*RFP-CreERT2*R26R*YFP reporter mice on d5 and d13 after infection with *N. brasiliensis*. Data are from one experiment are representative of at least two independent experiments.